

# 7 Element Strategy Initiative to Form Core Research Center for Electron Materials

– Multi probe study using X-rays, muons and neutrons –

*Youichi Murakami, Hiroshi Kumigashira,  
Kenji Kojima, Jun-ichi Yamaura*

## 7-1 Introduction

The national project "Elements strategy initiative to form core research center for electron materials" was started in 2012. Our objective is to develop entirely new materials based on ubiquitous elements. In this process, materials will be developed based on successful past experience, using approaches that are independent of development policy, by pioneering the developing of electronic materials to create new guidelines for material design using non-toxic elements to open up new fields in material science. We will be investigating the crystal, local, electronic, and magnetic structures of new functional materials using synchrotron radiation, muon and neutron sources.

## 7-2 Crystal structure under high-pressure in iron-based ladder superconductor $\text{BaFe}_2\text{S}_3$

The  $\text{AFe}_2\text{X}_3$  ( $\text{A} = \text{K}, \text{Rb}, \text{Cs}, \text{and Ba}$ ;  $\text{X} = \text{S}, \text{Se}, \text{and Te}$ ) series has a  $\text{CsCu}_2\text{Cl}_3$ -type structure with two-leg Fe ladders consisting of edge-shared  $\text{FeX}_4$  tetrahedral units. Hence, iron-based ladder materials are viewed as being closely related to this two-dimensional iron-based superconductor.

Recently, Takahashi *et al.* reported on pressure induced superconductivity in the iron-based ladder  $\text{BaFe}_2\text{S}_3$ .  $\text{BaFe}_2\text{S}_3$  behaves as an insulator throughout the entire temperature range at ambient pressure with a stripe type antiferromagnetic ordering at  $T_N = 110$  K. The application of pressure suppresses these ordered states, and superconductivity emerges immediately after vanishing  $T_N$  at 9 GPa. Eventually,  $T_c$  achieves a temperature of 24 K at 11.6 GPa.

In order to investigate the origin of supercon-

ductivity, synchrotron X-ray powder diffraction was performed at 300 K at NE1A of PF-AR, KEK. Pressure values up to ~12 GPa were applied using a diamond anvil cell. Two-dimensional X-ray images were collected by a RIGAKU R-Axis diffractometer with a curved imaging plate at a wavelength of  $\lambda = 0.420103$  Å. The crystal structures were determined using the Rietveld method.

We observed notable pressure effects: the large shrink of the Fe-ladder unit, the consider-

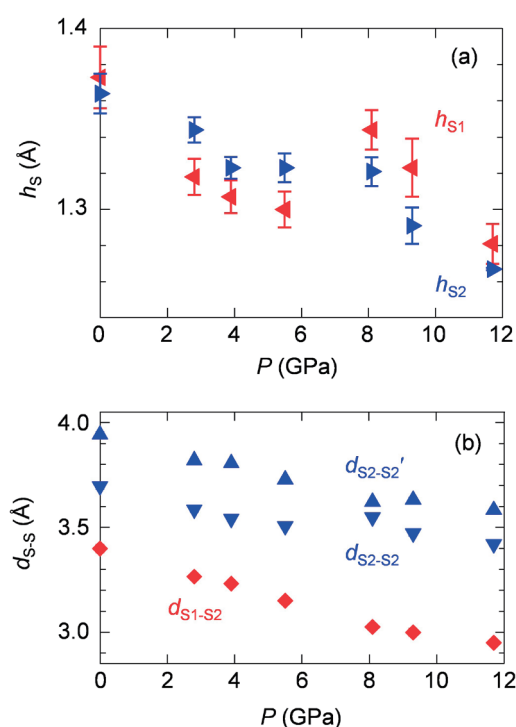


**Fig. 1:** (a) Pressure dependence of S atom height  $h_S$  from the Fe plane. The superconductivity emerges above 9 GPa after the suppression of the magnetically ordered state. (b) Pressure dependence of the S-S distance between neighboring ladder units  $d_{S1-S2}$ ,  $d_{S2-S2}$ , and  $d_{S2-S2'}$ .

able decrease in the S atom height, and significant enhancement of the S-S contact between the ladders. Representative parameters of the pressure dependence of the S atom height  $h_s$  from the Fe basal plane are plotted in Fig. 1(a). The significant decrease of  $h_s$  implies a large alteration of the electronic state. This may introduce the strong hybridization of Fe and S orbitals, resulting in the emergence of metallic behavior. Figure 1(b) shows the pressure dependence of the S-S contact. The large decreases of the  $d_{S-S}$  values suggest that the one-dimensionality of the sample is weakened by the application of pressure. The change in electronic correlations likely plays an active role in the emergence of superconductivity.

### 7-3 Inelastic neutron spectroscopy in the LaFeAsO<sub>0.9</sub>D<sub>0.1</sub> superconductor: Dynamics of interstitial hydrogen probing of the superconducting state

Hydrogen, with a light atomic mass is prone to exhibiting quantum effects such as tunneling motion at low-temperature. Neutron scattering is a powerful tool for probing hydrogen motion on the atomic scale because hydrogen displays enormous incoherent scattering. Tunneling is frequently examined theoretically by assessing the motion of hydrogen in a double-well potential that couples to the low-energy excitation modes of the metallic electrons.

We performed inelastic neutron scattering to investigate an iron-based superconductor LaFeAsO<sub>1-x</sub>D<sub>x</sub>. LaFeAsO<sub>1-x</sub>H<sub>x</sub> has a magnetic parent phase at  $x \sim 0$ . By substituting H<sup>-</sup> for O<sup>2-</sup>, namely doping electrons, a superconducting phase emerges with  $T_{c,max} = 26$  K at  $x \sim 0.08$  in place of the parent phase. Scattering laws  $S_D$  for the D-sample and  $S_F$  for the F-sample ( $x = 0.1$ ) were acquired using a chopper spectrometer (4SEASONS) at BL01 in the high-intensity pulsed-neutron source at MLF, J-PARC.

We observed pronounced concentrations of three flat-like bands at 6 K and diffuse scattering at 41 K. Meanwhile,  $S_F$  did not differ significantly between 6 K and 41 K. To visualize the difference between the D- and F-samples, Figures 2(a) and 2(b) show the difference maps  $S_{D-F}$ , which were obtained by subtracting the F-sample intensity from the D-sample intensity at 41 K and 6 K. The three peaks at  $\hbar\omega = 14.5$  (U), 11.0 (M), and 5.5

(L) meV at 6 K transform into strong quasi-elastic scattering centered at  $Q \sim 0$  meV at 41 K. We do not ascribe this to magnetic scattering because a rapid decrease of  $S_{D-F}$  with increasing  $Q$  would be observed, according to the squared magnetic form factor.

It is natural to consider that the immense  $S_{D-F}$  is intimately associated with the difference in the synthesis method between the two samples; namely, the implanted hydrogen gives rise to the strong excitation in the D-sample. Based on the two-site tunneling model with the interstitial hydrogen, we determined the tunneling matrix, the coupling constant of the hydrogen to the conduction electrons, the damping factor of the tunneling motion, the hydrogen quantity, and the tunneling distance as described in the literature [2].

Figure 2(c) displays the temperature dependence of the linewidth for the U- and M-modes. Notably,  $\hbar\Gamma_U$  and  $\hbar\Gamma_M$  rapidly grow in intensity at

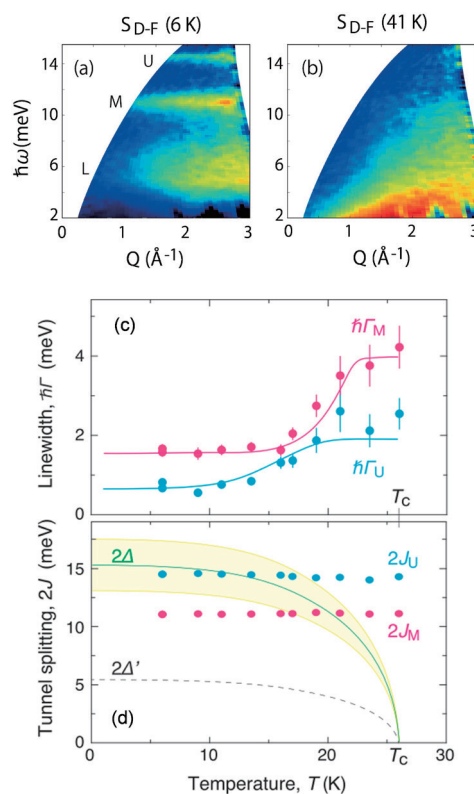


**Fig. 2:** Difference map  $S_{D-F}$  ( $S_D - S_F$ ) at 6 K (a) and 41 K (b). The U, M, and L denote the upper, middle, and lower modes. Temperature dependence of  $\hbar\Gamma_n$  (c) and  $2J_n$  (d). The blue and red solid lines are the calculated  $\hbar\Gamma_n(T)$ . The green solid line is the temperature evolution of the BCS-type gap formation  $2\Delta$  with its fitting distribution (yellow shaded area).  $2\Delta'$  (dash dotted line) indicates another superconducting gap reported in nuclear quadrupole resonance.

different temperatures. Figure 2(d) indicates plots of the temperature dependence of the tunnel splitting  $2J$ . The values are estimated to be  $J_U = 14.5$  meV for the U-mode and  $J_M = 11.0$  meV for the M-mode. The rapid growth of  $\hbar\Gamma$  is relevant to the different electronic states in the superconducting and normal states. The excitations of conduction electrons within the superconducting gap state ( $\hbar\omega < 2|\Delta(T)|$ ) are strongly suppressed, resulting in  $\hbar\Gamma \rightarrow 0$  with  $T \rightarrow 0$ . In contrast, when  $\hbar\omega > 2|\Delta(T)|$ , the tunnel oscillation is rapidly damped, namely,  $\hbar\Gamma_S$  switches to  $\hbar\Gamma_N$  when  $J_n$  and  $\Delta(T)$  cross. In this case, we assume that  $2\Delta(T)$  depends on the BCS-type thermal evolution with a Gaussian distribution, so we can reliably account for the rapid growth in intensities at different temperatures for  $\hbar\Gamma_U$  and  $\hbar\Gamma_M$ . In the fitting, we determined the tunnel splitting parameters at  $2J_U = 14.5$  meV and  $2J_M = 11.2$  meV. The estimated gap size is  $2\Delta_0 = 15.3$  meV (green curve) with 15%-distribution for  $2\Delta_0$  (yellow shaded region), as shown in Fig. 2(d).

This probe is a unique method and can easily allow gaps to be readily identified, assisted by the enormous incoherent scattering of hydrogen, although the superconducting gap exhibits very weak excitation.

#### 7-4 ARPES studies of $\text{Ca}_3\text{PbO}$ : Candidate material for 3D Dirac fermion system

Three-dimensional (3D) Dirac fermion systems are of great interest in condensed matter physics. These phenomena have been theoretically predicted and experimentally determined to occur at the phase transition point between a trivial insulator and a topological insulator, or in topological semi-metals including those of the 3D Weyl, 3D Dirac, and topological nodal line semi-metal. Recently, theoretical calculations have resulted in an interesting material: a cubic anti-perovskite  $\text{Ca}_3\text{PbO}$  which presents a 3D gapped Dirac-like cone at finite momentum.

The inverse perovskite  $\text{Ca}_3\text{PbO}$  crystallizes in the  $Pm\bar{3}m$  space group, cubic crystal system. The O atoms are located at the center of the unit cell, surrounded by corner-sharing, regular  $\text{Ca}_6$  octahedral. In order to identify the 3D massive Dirac fermions, we performed bulk-sensitive SX-ARPES measurements at the beam line BL-2A MUSASHI at KEK-PF. The experimental data were collected using a Scienta SES-2002 electron energy ana-

lyzer with linearly polarized light along the horizontal direction.

Figure 3(a) presents the result of the valence band structure along the X- $\Gamma$ -X path of the  $k_x$  axis with  $k_y = 0 \text{ \AA}^{-1}$ , along with plots of the peak positions of the momentum distribution curves (MDCs) and energy distribution curves (EDCs). The two Pb  $6p_{3/2}$  bands marked as B1 and B2 cross the  $E_F$  and consequently form hole pockets around the point. The presence of these hole pockets is in accord with the p-type behavior observed in transport measurements. The experimental result is in good agreement with the band calculation as shown in Fig. 3(a). The agreement between the modified calculated bands and the APRES spectra is further confirmed by the close match between the second-derivative ARPES spectra and the calculations in Fig. 3(b). These findings imply that the  $\text{Ca}_3\text{PbO}$  is a candidate material for native 3D Dirac fermions.

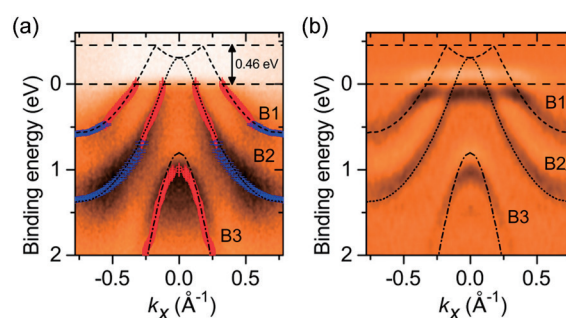


**Fig. 3:** (a) ARPES intensity along the  $\Gamma$ -X lines of the  $k_x$  directions. The peak positions of the MDCs and EDCs are represented by the red open squares and blue open circles, respectively. Black dashed lines represent the results of band structure calculations. (b) Second derivative ARPES spectra along the  $\Gamma$ -X lines of the  $k_x$  directions.

#### 7-5 Development of general purpose $\mu\text{SR}$ spectrometer ARTEMIS at S1 experimental area, MLF J-PARC

A new  $\mu\text{SR}$  spectrometer "ARTEMIS" was developed and installed at the S1 experimental area of MLF, J-PARC [4]. This general purpose spectrometer is identical in design to the D1-spectrometer developed in 2013. The common design of the two spectrometers facilitates sharing of the sample environment and direct comparison of the beam characteristics. We upgraded the front-end circuit of the positron and electron detectors,

which enables the detection of high hit-rate tolerance from muon beams even for 1 MW operation of MLF.

### References

- [1] Crystal structure determination under high-pressure in iron-based ladder superconductor  $\text{BaFe}_2\text{S}_3$ , K. Kobayashi, S. Maki, Y. Murakami, Y. Hirata, K. Ohgushi, and J. Yamaura, to appear in *Supercond. Sci. Technol.*
- [2] Inelastic neutron spectroscopy to examine the dynamics of interstitial hydrogen in the iron-based  $\text{LaFeAsO}_{0.9}\text{D}_{0.1}$  superconductor, H. Hiraka, J. Yamaura, S. Iimura, Y. Muraba, K. Ikeuchi, M. Nakamura, Y. Inamura, R. Kajimoto, T. Honda, M. Hiraishi, K. M. Kojima, R. Kadono, Y. Murakami, K. Yamada, S. Matsuishi, and H. Hosono, submitted to *Phys. Rev. B*.
- [3] ARPES studies of the inverse perovskite  $\text{Ca}_3\text{PbO}$ : Experimental confirmation of a candidate 3D Dirac fermion system, Y. Obata, R. Yukawa, K. Horiba, H. Kumigashira, Y. Toda, S. Matsuishi, and H. Hosono, *Phys. Rev. B* **96**, 155109 (2017).
- [4] Development of general purpose  $\mu\text{SR}$  spectrometer ARTEMIS at S1 experimental area, MLF J-PARC, K. M. Kojima, M. Hiraishi, A. Koda, H. Okabe, S. Takeshita, H. Li, R. Kadono, M. M. Tanaka, M. Shoji, T. Uchida, and S. Y. Suzuki, *JPS Conf. Proc.*, **21** 011062 (2018).